

Electrothermal Modeling and Characterization of High Capacity Lithium-Ion Battery Systems for Mobile and Stationary Applications

M. Giegerich, S. Koffel, R. Filimon, J.L. Grosch, T. Fühner, M.M. Wenger, M. Gepp, V.R.H. Lorentz
Fraunhofer IISB, Erlangen, Germany
vincent.lorentz@iisb.fraunhofer.de

Abstract - In mobile and stationary battery systems, lifetime expectancy is a key parameter for the calculation of monetary effectiveness. It significantly affects return on investment and therefore is a key parameter for the market breakthrough of the desired battery application. Battery life is influenced by two different factors, namely electrical utilization and environmental conditions. As higher temperatures lead to a faster deterioration of the lithium-ion battery, smart thermal design can not only increase battery lifetime, but also reduce cooling costs and improve overall efficiency. It is therefore essential to establish an effective thermal design through performing electrothermal modeling and characterization of the battery cell, battery module and fully assembled battery pack. In this paper, the motivation for electrothermal modeling of lithium-ion battery cells and modules is introduced and design challenges are identified for applications in mobile and stationary battery systems. An electrothermal model of batteries with appropriate cell chemistry for mobile and stationary applications is developed with focus on further implementation in thermal simulation of battery modules and packs. The parameterization process of the presented models is shown and a model of battery cells with derived parameters is presented. Finally, the electrothermal model is verified experimentally.

I. INTRODUCTION AND MOTIVATION

A. Temperature Dependent Battery Models

A battery system should be able to estimate its own state, protect itself against failure and degradation, and provide information about its state to other system components, e.g. to a driver's user interface in electric vehicles or to a power utility in stationary applications.

To predict valuable information such as remaining driving distance, state of charge (SOC) and others, various battery models can be used. Correction and adaption of these models can be applied by different filters like the extended Kalman filter (EKF) [1][2] and other variations of the Kalman filter [3][4]. The parameters for the models are significantly dependent on temperature. Exact thermal characterization leads to more accurate estimations of SOC and all temperature dependent indicators.

B. Battery Degradation Induced by Temperature

Lithium-ion batteries lose capacity when electric charge is transferred and also while they are simply being stored.

Operational parameters such as maximum current limits, number of cycles, cycle depth and internal heat generation along with thermal parameters as ambient temperature and cooling strategies together all have an impact on battery lifetime.

Loss of capacity due to charging and discharging of the battery influences the so called cyclic lifetime. Capacity losses related to specific ambient parameters such as temperature and storage time are called calendric losses. The indicator of overall capacity loss in a battery is called its state of health (SOH) and can be defined as ratio of actual capacity Q_{act} to initial capacity $Q_{initial}$. Consequently, SOH can be divided into SOH_{cyclic} , which is a function of transferred charge, and $SOH_{calendric}$, which is a function of temperature and time.

The calendric lifetime is mainly determined by the time and the temperature of the cell since the internal processes are of chemical nature and thus follow the Arrhenius equation [5]. This equation describes the dependency of reaction kinetics (i.e., battery cell aging) in relation to temperature (i.e., battery temperature). Foresighted thermal design is obligatory to minimize a battery's rate of degradation.

II. CHALLENGES OF THERMAL DESIGN

The foremost aim for the thermal design of a battery system should be to minimize temperature gradients while delivering sufficient cooling power to dissipate heat generated during battery operation. Temperature differences between cells inside modules and packs lead to variances in all temperature dependent processes, especially leading to unequal aging and self-discharge rates. With the resulting capacity variation, more battery cell voltage balancing effort is required and the overall efficiency decreases.

Thermal design optimization has to be broken down into local domains:

- low temperature gradients across cell
- low temperature gradients across module
- low temperature gradients across pack

To provide sufficient cooling power, different strategies can be used, namely air and liquid cooling. Liquid cooling can transport and dissipate more energy than air cooling, but

liquid cooling systems are more complex and are thus more costly.

To define the optimum operating temperature of the battery, a tradeoff has to be made. On the one hand lithium-ion batteries can deliver significantly higher currents when operated at higher temperatures. This can be explained by a drop in internal resistances and is described in the following section. On the other hand, the cells undergo increased degradation at higher temperatures and will consequently reach their end-of-life earlier.

The type of temperature sensor, their number and position should also be part of the thermal design. The current trend is to reduce the number of temperature sensors inside battery modules to lower costs. Though this has the advantage of reducing packaging and cabling complexity, but it has the disadvantage of losing the possibility to determine every battery cell's individual temperature. A possible approach to reduce costs while still enabling temperature measurements on every cell, is to integrate printed temperature sensors on foils or directly onto the battery package as shown in Fig. 1. This sensor is based on the development presented in [6].

The positioning of the foil based temperature sensor is also a sensitive point in the design of a battery system. In high-power applications requiring battery cells providing high C-rates (i.e., current peaks above 5C), like hybrid electric vehicle (HEV) or electric sports cars, hotspots can occur inside the battery or at the battery electrodes and connectors. These hotspots can result in faults that either go undetected or are detected too late and lead to a thermal runaway of batteries with certain lithium-ion chemistries. It therefore represents a safety risk when a temperature sensor is not positioned at the hottest location (i.e., in general the positive electrode of the pouch cells). On the other hand, error is introduced into the calculation of the temperature dependent parameters such as SOC when using hotspot temperatures instead of average temperatures.

After this introduction of the challenges present in the thermal design of battery systems, an overview of the methods used for both electric and thermal modeling will be presented hereafter.

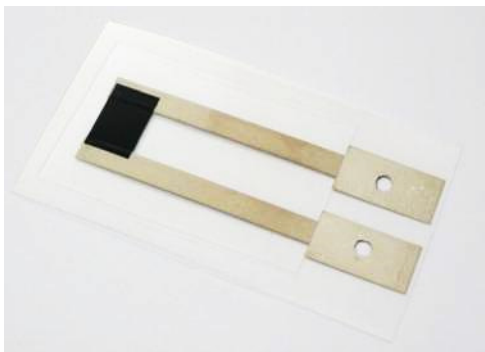


Fig. 1: Photography of a temperature sensor printed on foil

III. ELECTROTHERMAL MODELING

State-of-the-art battery models can follow different approaches [7]. Electrothermal battery models are often split into an electrical and thermal model [8]. In the following, they are described separately first and their coupling is discussed subsequently.

A. Electrical Modeling

For electrical modeling of battery cells, equivalent networks are mainly used. Lumped elements of the equivalent networks can be of electrical nature (e.g., resistors, capacitance, inductor, voltage and current sources) or describe chemical effects, like diffusion in the active material (e.g., constant phase element, Warburg impedance, Nernst impedance). In Fig. 2, a typical electrical equivalent circuit model is shown. It comprises a voltage source V_0 , an internal resistance R_i and one or more RC circuits [9]. The accuracy of the model can be improved by using more RC circuits, but often just one is used due to the parameterization effort and the required computing power [10]. This first RC circuit models the most significant process in the battery: the intrinsic electrochemical double layer capacitance that is present in every lithium-ion battery due to the electrode-electrolyte interface. Additionally, a resistor R_{sd} representing the self-discharge of the battery can be added. The self-discharge process of a battery is voltage, time and temperature dependent, thus making the parameterization of this resistor difficult. However, self-discharge of the cell can be neglected in most power applications and in systems dominated by the standby energy consumption of the battery monitoring electronics.

Various methods for the parameterization of the electrical equivalent circuit can be used. Besides electrochemical impedance spectroscopy (EIS) [11] and a numerical approach using hybrid power pulse characterization (HPPC), other methods like the current step response method or the current interrupt method are also possible.

EIS was used in a first approach for the characterization of the battery cell and parameterization of the equivalent circuit model. Nyquist plots of various EIS measurements at different temperatures can be seen in Fig. 3. The measurements were performed with high precision measurement equipment, in this case a Gamry Reference 3000 potentiostat. When characterizing low impedance

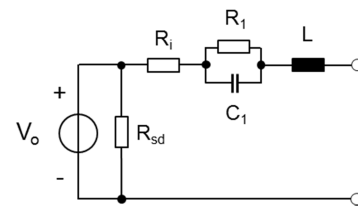


Fig. 2: Electrical equivalent circuit representing a lithium-ion battery cell

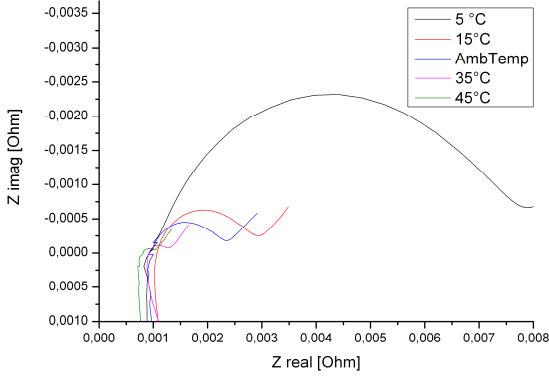


Fig. 3: Nyquist plot for EIS spectra of LFP cell at 50% SOC and at different temperatures

materials such as high capacity lithium-ion pouch cells, a booster has to be used in order to have a higher stimulus current and therefore to measure an utilizable voltage response. To perform measurements at different temperatures, aluminum plates with liquid flowing within at the desired temperature were used.

The frequency range of the spectra for battery material analysis typically ranges from 10 kHz down to 10 mHz. Above 10 kHz, the inductive behavior of the measurement feed lines is dominant even in a four-wire system with shielded cables.

In Fig. 3, the spectra of the measurement of a 45 Ah pouch cell with lithium iron phosphate (i.e., LiFePO_4 , LFP) chemistry are shown. At the point of the zero-crossing of the x-axis, the real part of the impedance indicates the internal resistance R_i . The half circle at lower frequencies represents the electrochemical double layer or the RC part of the equivalent circuit, respectively. Parameter optimization of the equivalent circuit can be done with a Levenberg-Marquardt algorithm for nonlinear least square optimization.

B. Electrical Parameterization

Since the EIS method does not give information on V_0 , which is essential for determining SOC in state space models used in EKF, V_0 has to be modeled separately. This is a challenging task, because of the temperature dependence of the SOC and other effects such as hysteresis of the open circuit voltage (OCV) [12][13][14] or the series resistance R_i [15]. The variation of the OCV with temperature is related to a change in entropy [16] and a measurement with a 45 Ah LFP pouch cell can be seen in Fig. 4. The same cell was also used for the measurement of the OCV variation with different states of charge that can be seen in Fig. 5. This figure shows only 140 mV variation between the fully charged state and the fully discharged state.

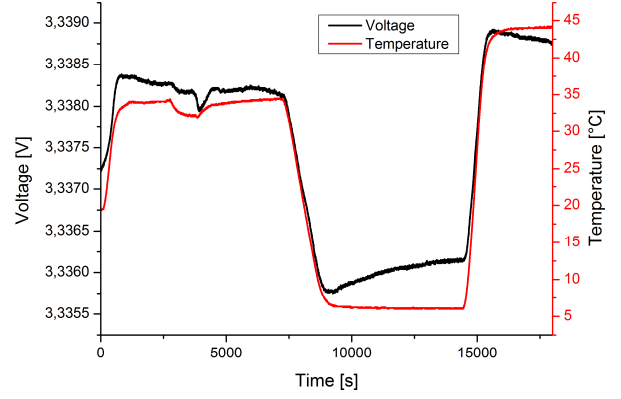


Fig. 4: OCV variation with different temperatures

A first approach with simple averaging charge and discharge curves at very low currents (i.e., C/20 rate) showed insufficient results and thus HPPC measurements were performed, according to Dynamic Discharge Power Profile B in the ISO/DIS 12405-2 [17] (see Fig. 6). These measurements were then used to correctly parameterize a Thévenin model by minimizing the misfit between measured and simulated data. The measurement and the corresponding simulated voltage curve can be seen in Fig. 7. The parameters of the replacement model served as optimization variables. Since even this simplistic model can be expected to broadly capture the physical behavior of the battery, there is at least one solution to the error minimization problem that actually reflects the state of the battery that corresponds to the measured terminal voltages under the given charge/discharge cycle. Under this assumption, the optimized model parameters adequately describe the non-measurable data of the battery. However, this methodology constitutes an ill-posed problem in which there exist many different solutions that minimize the misfit error. From an optimization perspective, the search space exhibits a high number of local

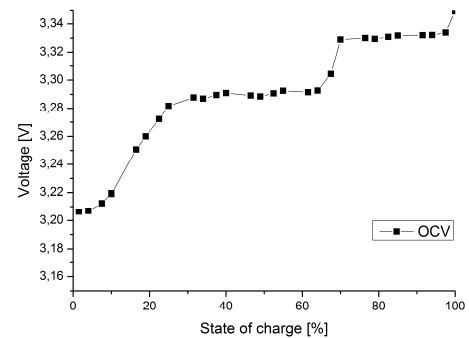


Fig. 5: Open circuit voltage variation with different SOC after 12 hour relaxation at 20 °C

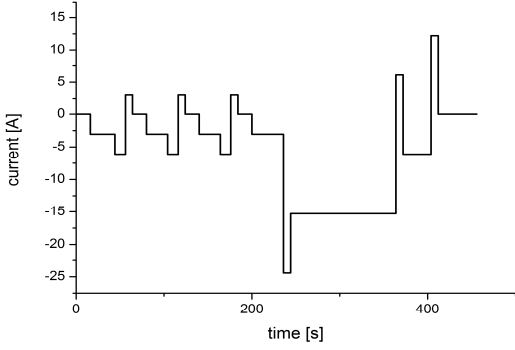


Fig. 6: Single cycle of HPPC current profile according to [17]

optima from which the one that most closely resembles the physical behavior has to be selected. A number of approaches for these situations are available, including regularization frameworks [18] or rigorous constraint formulations to exclude non-viable solutions.

Another issue is the selection of an appropriate search strategy. The majority of numerical optimizers, for example, strongly depend on the selected initial guess: different start values lead to different final minimization solutions. Global optimizers, on the other hand, are well suited to simultaneously explore large areas of the search space. Often, however, they fail to intensively exploit local information such as gradients. Thus, a hybrid approach in which the entire search space is broadly scanned followed with the obtained sub-optima being used as start values for a thorough local search, can be considered an adequate approach, similarly to what has been proposed by [19]. In this work, a multi-objective genetic algorithm was applied [20], with the misfit error as the first optimization target and the constraint violation value as the second. A first-order RC model without accounting for hysteresis was used in this first stage. Constraints were formulated such that only realistic

resistances ($0 \Omega < R_i < 4 \text{ m}\Omega$) and open-circuit voltages ($0 \text{ V} < V_0 < 5 \text{ V}$) were permitted. Additionally, V_0 start values were obtained through an equilibrium charge/discharge cycle. These values were used as “seeds” for the genetic algorithm. After approximately 1500 iterations (50 candidate solutions per iteration), a number of solutions that represent a compromise between constraint violation and minimum error were achieved. From this set of solutions, one or two promising candidates were extracted and taken as initial guesses for the second stage, a local optimization step. In the scope of this work, we have experimented with different numerical optimizers and found that a sequential least-squares and a trust-region sequential quadratic programming [21] approach showed the best performance. Both methods are suited for non-linear programming problems with equality and inequality constraints. The same constraints as for the global optimization step but without hysteresis were considered for this stage. An intensive search yielding close fits between measured and simulated data was conducted. In order to account for hysteresis, the final solutions were refined during a third optimization stage. The hysteresis was considered through an extended Thévenin model [22] in which both the open circuit voltage and the RC-network resistances were separated into a charge and discharge component.

C. Thermal Modeling and Parameterization

Thermal modeling can be performed with the help of finite element methods (FEM). A detailed CAD model of the battery cell is created with CAD software and parameterized with the appropriate thermal parameters, namely thermal conductivity and specific heat. As the complete geometry of the battery cell is considered, detailed boundary conditions can be defined, to describe the cooling conditions used. The specific losses are applied to the geometry on the appropriate elements. The model was simulated using the ANSYS framework.

The losses are not constant and depend on both the temperature of the cell and its state of charge. As a consequence, it is necessary to use a coupled simulation to be able to take into account the influence of the temperature on both the internal resistance of the battery and accordingly that of the losses. The issue is that such FEM simulations are very time consuming. A solution to this issue is the use of model order reduction (MOR). A large scale dynamic system of the first order is described as

$$E \dot{\mathbf{x}} = A \mathbf{x} + B \mathbf{u} \quad (1)$$

$$\mathbf{y} = C \mathbf{u} \quad (2)$$

where A and E are the system matrices, B the input matrix and C the output matrix. \mathbf{x} is the state vector of the system, \mathbf{u} is the input of the system and \mathbf{y} the output. The aim of MOR as stated in [23] is to generate a low-dimensional approximation in the form

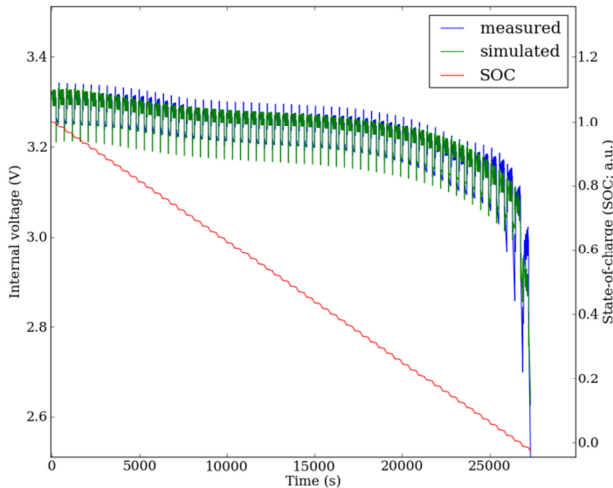


Fig. 7: Voltage and SOC Measurement of HPPC cycle and simulated voltage with equivalent circuit model

$$E_r \dot{z} = A_r z + B_r u \quad (3)$$

$$y = C_r z \quad (4)$$

which describes the dependence of y on u while the dimension of the reduced state vector z is much smaller than the dimension of the original state vector x . MOR was used with the software mor4ansys as described in [23].

Fig. 8 compares the results of the reduced model with the results of the FEM model for the simulated mean temperature on the electrode stack. For these simulations, constant power losses were considered up to a time of 1000 s: 20 W on the electrode stack, 1 W on the aluminum tab and 0.8 W on the copper tab. The cell then cooled down over 1000 s. The results were very similar, with a temperature difference less than 0.1 °C, except that the computation time had been reduced: The simulation of the FEM model with 54342 nodes and a maximum time step of 1 s took 3859 s, while the reduced simulation took 8 s. The simulation time ratio is then 482:1. With this reduced model, it is possible to make a coupled simulation with the electric model.

The reduced model allows simulating the mean temperature over the electrode stack but does not give information about temperature gradients. This issue can be circumvented by using the transformation matrix: this matrix is used to transform the original system into the reduced system but this can also be used for the inverse transformation. To demonstrate this, the inverse transformation was applied to the reduced system for a time of $t=1000$ s. Fig. 9 shows the comparison between the temperature distribution obtained with the FEM and the inverse transformed reduced model, along with the temperature difference between both temperature distributions. The maximum difference is 0.03 °C, showing that the reconstructed temperature distribution is accurate compared to the FEM simulation and allows analysis of the temperature gradients.

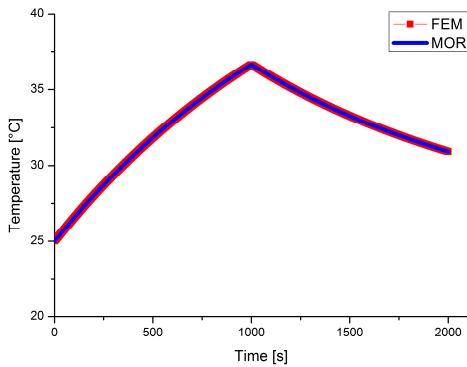


Fig. 8: Comparison of the mean temperature of electrode stack simulated with FEM and with MOR: deviation is below 0.1 °C

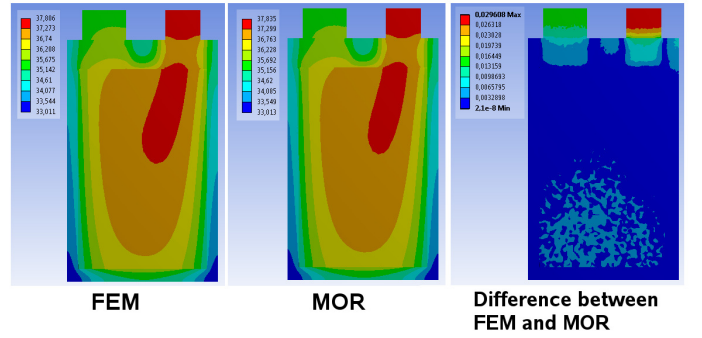


Fig. 9: Comparison of the simulated temperature distribution obtained with the FEM simulation and MOR.

D. Coupling of the Electrical and Thermal Models

Once the electrical model and the reduced thermal model have been obtained, a coupled simulation can be made with the procedure shown in Fig. 10. The current profile is the input of the model, with the initial state-of-charge. For each time step, the evolution of the state of charge is calculated and the temperature of the electrode stack is obtained from the reduced thermal model. The dependence of the series resistance on state of charge and on temperature was determined in the part on the determination of the electrical model. With this data, the series resistance R_s of the batteries is determined. Using the current value I , the dissipation in the electrode stack is determined with $R_s \cdot I^2$. This dissipation value is fed into the reduced thermal model which returns the mean temperature of the battery stack for the next time step. The procedure is then repeated.

A current profile with discharging at constant current was used as input for the coupled model. The evolution of the system was simulated and the temperature distribution was extracted at the end of the current profile. The result is shown in Fig. 11. In the next section, these simulation results will be compared with measurements.

IV. EXPERIMENTAL RESULTS

The measurement setup consists of a single pouch type battery cell of 45 Ah capacity, a high-current bidirectional

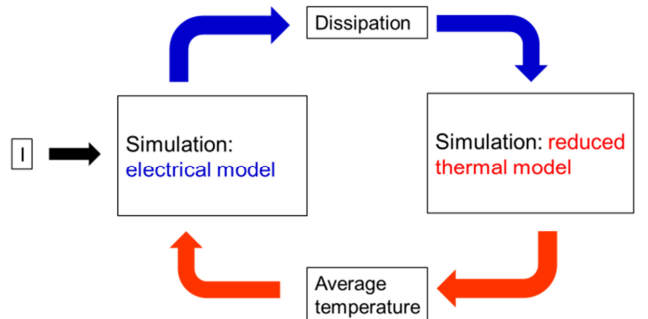


Fig. 10: Principle of the coupled electro-thermal simulation.

source-sink, an infrared camera of type Flir E50 for image acquisition and 18 thermocouples of type K connected to a data logger. The thermocouples are placed in a grid pattern on the battery cell, whereby one side was left unpopulated for the recording of the infrared radiation.

In order to provide the same ambient and cooling conditions for both, experimental measurements and simulations, a floating cell measurement setup was chosen, as shown in Fig. 12. Considering this setup, natural convection is expected to be the dominant mechanism for heat transfer between the cell and its environment. Measurements are performed with constant current of 45 A (1 C discharge rate) for discharging the battery cell. The measurements of thermal radiation (by the infrared camera) and local surface temperature (by the thermocouples and data logger) were recorded synchronously for better comparison. The thermocouples were used to check the temperatures measured by the infrared camera. The results shown in Fig. 11 were obtained by simulating with the same time and current used for the measurements and recovering the temperature distribution at the end of the discharge process.

By comparing Fig. 11 and Fig. 12, it can be seen that the coupled simulation allows the behavior of the system to be described, as the simulated temperature distribution is very close to the measured one. A quantitative comparison between thermocouple (TC) and simulation at specific measurement locations is shown in Table I.

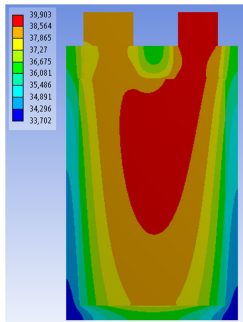


Fig. 11: Temperature distribution obtained after the coupled electrothermal simulation with the reduced thermal model.

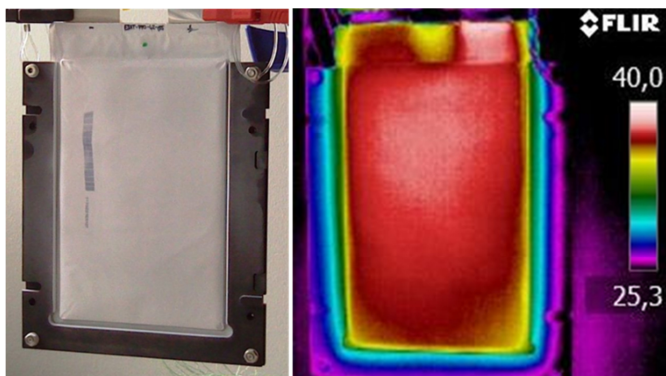


Fig. 12: Picture of the floating cell measurement setup (left) and infrared recording in the end of the discharging process (right).

TABLE I:
COMPARISON OF TEMPERATURE MEASUREMENT AT SPECIFIC POINTS OF
45AH CELL

Thermocouple position	Measurement TC [°C]	Simulation [°C]	ΔT [°C]
Below neg. tab	37,9	38,8	0,8
Center below tabs	35,5	36,6	1,1
Below pos. tab	37,3	38,0	0,7

V. CONCLUSION AND OUTLOOK

In this paper a complete process of coupled electrothermal modeling and simulation was presented. A simplified process visualization is synthesized in Fig. 13.

In this process the possibilities to determine the parameters of the electrical models were presented and it was shown that HPPC combined to appropriate optimization methods allowed the experimental results to be described. The benefits of model order reduction for the thermal model were shown. In contrary to FEM, it allows fast simulations to be carried out, is suited for electrothermal coupling, while enabling temperature gradients at desired time steps to be obtained. The coupled electrothermal simulation was then performed. This result was compared to measurements of a 45 Ah lithium-ion cell with LFP cell chemistry. Further, the measurement setup was presented. The simulation of the coupled electrothermal model presented in this paper shows a very good accordance with the experimental results. It was shown that the proposed method for electrothermal modeling allows simulating complex battery systems accurately and without requiring huge computational power, thus enabling improvements of cooling and heating systems in the conception phase of mobile and stationary battery powered applications, before costly fabrication and tests.

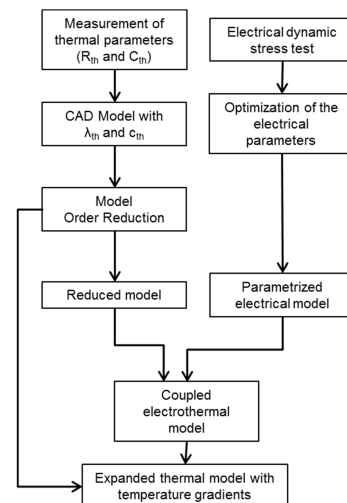


Fig. 13: Process description of electrothermal modeling and simulation

ACKNOWLEDGMENT

The research leading to these results has received funding as part of the Energie Campus Nürnberg ("EnCN") which is financed by the State of Bavaria as part of the program Bavaria on the move, and the SEEDs project which is funded by the Bavarian State Ministry of Economic Affairs, Infrastructure, Transport and Technology in the framework of the Bavarian initiative for research and development of technology in the energy sector. Also funding was received from the European Union Seventh Framework Program (FP7/2007-2013) under grant agreement n°285224 ("SuperLIB") and grant agreement n°314128 ("AVTR").

The authors thank Mika Räsänen (former European Batteries Oy in Finland) for his support by providing battery cell components and fruitful discussions.

REFERENCES

- [1] Hussein, H.A.-H.; Batarseh, I., "State-of-charge estimation for a single Lithium battery cell using Extended Kalman Filter", *2011 IEEE Power and Energy Society General Meeting*, 24-29 July 2011
- [2] G. Plett, "Extended Kalman Filtering for Battery Management Systems of LiPB-based HEV Battery Packs. Part 1. Background.", *Journal of Power Sources* 134 (2004), pp. 252-261. 2004
- [3] Pu Shi; Yiwen Zhao; Pu Shi, "Application of Unscented Kalman Filter in the SOC Estimation of Li-ion Battery for Autonomous Mobile Robot," *2006 IEEE International Conference on Information Acquisition*, pp.1279-1283, 20-23 Aug. 2006
- [4] Hongwen He; Rui Xiong; Xiaowei Zhang; Fengchun Sun; JinXin Fan, "State-of-Charge Estimation of the Lithium-Ion Battery Using an Adaptive Extended Kalman Filter Based on an Improved Thevenin Model," *IEEE Transactions on Vehicular Technology*, vol.60, no.4, pp.1461-1469, May 2011
- [5] Vetter, J.; Novák, P.; Wagner, M.R.; Veit, C.; Möller, K.-C.; Besenhard, J.O.; Winter, M.; Wohlfahrt-Mehrens, M.; Vogler, C.; Hammouche, A., "Ageing mechanisms in lithium-ion batteries," *Journal of Power Sources*, vol. 147, Issues 1-2, 9 September 2005, Pages 269-281,
- [6] Lorentz, V. R H; Wenger, M. M.; Grosch, J. L.; Giegerich, M.; Jank, M. P M; März, M.; Frey, L., "Novel cost-efficient contactless distributed monitoring concept for smart battery cells," *2012 IEEE International Symposium on Industrial Electronics (ISIE)*, 28-31 May 2012
- [7] Gerschler, J.B.; Kirchhoff, F.N.; Witzhausen, H.; Hust, F.E.; Sauer, D.U., "Spatially resolved model for lithium-ion batteries for identifying and analyzing influences of inhomogeneous stress inside the cells," *IEEE Vehicle Power and Propulsion Conference, 2009. VPPC '09.*, pp. 295-303, 7-10 Sept. 2009
- [8] Baronti, F.; Fantechi, G.; Leonardi, E.; Roncella, R.; Saletti, R., "Effective modeling of temperature effects on lithium polymer cells," *Electronics, Circuits, and Systems (ICECS), 2010 17th IEEE International Conference on*, pp.990,993, 12-15 Dec. 2010
- [9] He, H.; Xiong, R.; Guo, H.; Li, S., "Comparison study on the battery models used for the energy management of batteries in electric vehicles", *Energy Conversion and Management*, vol. 64, pp. 113-121, December 2012,
- [10] Hu, S.; Li, S.; Peng, H., "A comparative study of equivalent circuit models for Li-ion batteries", *Journal of Power Sources*, vol. 198, pp. 359-367, 15 January 2012
- [11] Macdonald, J. R.; Barsoukov, E., "Impedance Spectroscopy – Theory, Experiment and Applications", Hoboken, N.J., Wiley-Interscience, 2005
- [12] Roscher, M. A.; Sauer, D. U., "Dynamic electric behavior and open-circuit-voltage modeling of LiFePO₄-based lithium ion secondary batteries", *Journal of Power Sources*, vol. 196, pp. 331-336, 1 January 2011
- [13] Roscher, M. A.; Bohlen, O.; Vetter, J., "OCV Hysteresis in Li-Ion Batteries including Two-Phase Transition Materials," *International Journal of Electrochemistry*, vol. 2011, Article ID 984320, 6 pages, 2011.
- [14] Eichi, H.R.; Mo-Yuen Chow, "Modeling and analysis of battery hysteresis effects," *2012 IEEE Energy Conversion Congress and Exposition (ECCE)*, pp.4479,4486, 15-20 Sept. 2012
- [15] Roscher, M. A.; Vetter, J.; Sauer, D. U., "Characterisation of charge and discharge behaviour of lithium ion batteries with olivine based cathode active material, *Journal of Power Sources*, vol. 191, Issue 2, pp. 582-590, 15 June 2009
- [16] Sato, N., "Thermal behavior analysis of lithium-ion batteries for electric and hybrid vehicles", *Journal of Power Sources*, vol. 99, pp. 70-77, August 2001
- [17] ISO/DIS 12405-2, "Electrically propelled road vehicles – Test specification for lithium-ion traction battery systems – Part2: High energy applications", International Organisation for Standardization, 2010
- [18] Tikhonov, A. N.; Arsenin, V. Y., "Solution of Ill-posed Problems" Washington: Winston & Sons., 1977
- [19] Hu, S.; Li, S.; Peng, H.; Sun, F. "Robustness analysis of State-of-Charge estimation methods for two types of Li-ion batteries", *Journal of Power Sources*, vol. 217, pp. 209-219, 1 November 2012
- [20] Zitzler, E.; Laumanns, M.; Thiele, L., "SPEA2: Improving the strength pareto evolutionary algorithm for multiobjective optimization," *Evolutionary Methods for Design Optimization and Control with Applications to Industrial Problems*, pp. 95--100. Athens, Greece, International Center for Numerical Methods in Engineering, 2001
- [21] Nocedal, Jorge, Wright, Stephen., "Numerical Optimization." 2nd ed., 2006
- [22] Jonghoon Kim; Gab-Su Seo; Changyoon Chun; Bo-Hyung Cho; Seongjun Lee, "OCV hysteresis effect-based SOC estimation in extended Kalman filter algorithm for a LiFePO₄/C cell," *2012 IEEE International Electric Vehicle Conference (IEVC)*, pp.1.5, 4-8 March 2012
- [23] E. B. Rudnyi, J. G. Korvink, "Model Order Reduction for Large Scale Engineering Models Developed in ANSYS", *Applied Parallel Computing. State of the Art in Scientific Computing, Lecture Notes in Computer Science*, vol. 3732, pp. 349-356, 2006